THE HONEYCOMB SUPERNOVA REMNANT

YOU-HUA CHU AND JOHN R. DICKEL
Astronomy Department, University of Illinois at Urbana—Champaign, Urbana, Illinois 61801
Electronic mail: chu@dorado.astro.uiuc.edu, johnd@sirius.astro.uiuc.edu

LISTER STAVELEY-SMITH
Australia Telescope National Facility, CSIRO, Box 76, Epping, New South Wales 2121, Australia
Electronic mail: lstavele@atnf.csiro.au

JÜRGEN OSTERBERG
Radioastronomisches Institut der Universität Bonn, Auf dem Hügel 71, D-53111 Bonn, Germany
Electronic mail: josterb@astro.uni-bonn.de

R. CHRIS SMITH
Cerro Tololo Inter-American Observatory,[1] Casilla 603, La Serena, Chile
Electronic mail: csmith@noao.edu

Received 1994 September 30; revised 1994 December 23

ABSTRACT

At 2.5 southeast of SN 1987 A, the Honeycomb Nebula is named after its interesting morphology, which consists of over ten loops with sizes of 2–3 pc. High-dispersion spectra of these loops show hemispheres expanding toward the observer at 100–300 km s^{-1}. Using archival X-ray data and a combination of new and archival radio data, we find bright X-ray and nonthermal radio emission associated with the Honeycomb Nebula. New CCD images further show enhanced [S II]/Hα ratios. These results confirm a model in which the Honeycomb Nebula is due to a supernova shock front, traveling toward the observer, encountering an intervening sheet of dense, but porous, interstellar gas. The bulk of the supernova remnant resides in a low-density cavity, and is not otherwise visible. The situation is similar to the hidden supernova remnants postulated for the X-ray bright superbubbles. The Honeycomb Nebula has an unusually steep radio spectral index ($S_\nu \propto \nu^{-1.2}$), normally associated with young SNRs.

1. INTRODUCTION

The Honeycomb Nebula was discovered serendipitously in a high-resolution Hα image centered on SN 1987 A, taken with the ESO New Technology Telescope (Wang 1992). The name "Honeycomb" was inspired by the nebular morphology, which contained more than ten loops with sizes of 7″–12″, or 2–3 pc for a distance of 50 kpc to the Large Magellanic Cloud (LMC). This peculiar morphology prompted considerable interest in this nebula.

To determine the origin and nature of the Honeycomb Nebula, Meaburn *et al.* (1993, 1995) obtained high-dispersion échelle observations, and found that the "loops" of the Honeycomb were the projected boundaries of hemispheres expanding toward the observer at V_{exp}~100–300 km s^{-1}. After considering and excluding the possibilities of multiple supernova remnants (SNRs) or Wolf–Rayet bubbles, they concluded that the Honeycomb Nebula was formed by one or more SNR shocks colliding with a lumpy, ambient sheet of gas.

Since the Honeycomb Nebula is only 2.5 southeast from SN 1987 A, X-ray or radio images of the ever-popular latter usually include the former. We find from archival data that the Honeycomb Nebula emits diffuse, soft X rays; it is also a source of nonthermal synchrotron radiation in the radio. We have obtained new radio observations to determine its radio spectral index, and CCD images in four filters to study its spectral properties and relationship with the ambient nebulosities. In this paper we analyze these data, report the results, and present a possible scenario for the formation of the Honeycomb Nebula. We will also discuss its complex interstellar environment.

2. X-RAY PROPERTIES OF THE HONEYCOMB NEBULA

The Honeycomb Nebula was detected by the Imaging Proportional Counter (IPC) of the *Einstein Observatory* (Source 536.2-6921 reported by Wang & Helfand 1991). It was also detected in recent *ROSAT* observations by both the Position Sensitive Proportional Counter (PSPC) and the High Resolution Imager (HRI). The *ROSAT* PSPC, sensitive in an energy range of 0.1–2.4 keV, has an on-axis resolution of 30″ and a spectral resolution of ~45% at 1 keV (Pfeffermann *et al.* 1987). The *ROSAT* HRI is an imaging instrument with a spatial resolution of 5″–6″ near the field center. The 27 000 s PSPC observation rp500100 (PI—Gorenstein) and the 23 500 s HRI observation wh400056 (PI—Hasinger) are

[1]Cerro Tololo Inter-American Observatory is part of the National Optical Astronomy Observatories (NOAO), which are operated by the Association of Universities for Research in Astronomy, Inc. under cooperative agreement with the National Science Foundation.

 0004-6256/95/109(4)/1729/6/$0.90

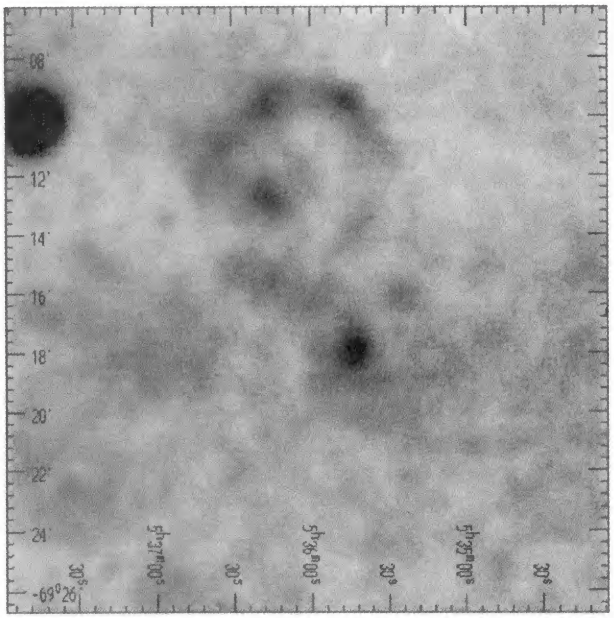

(a)

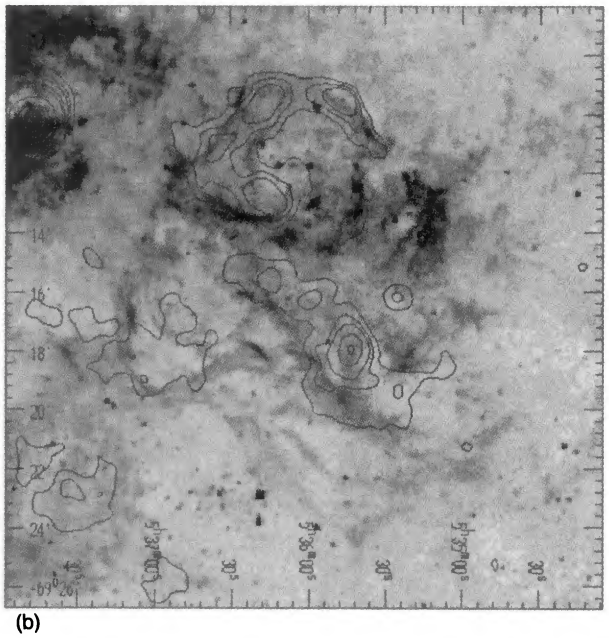

(b)

FIG. 1. (a) X-ray image and (b) Hα image with X-ray overlay of the Honeycomb Nebula. The field of view is 20.5×20.5. The X-ray picture is a smoothed PSPC image in the energy band of 0.1–2.4 keV. The Hα image is reproduced from a PDS scan file of a Curtis Schmidt plate. The X-ray contours are plotted at 3, 4, 5, 7.5, 10, 25, 50, 75, and 90% levels of 30 Dor B's peak intensity in the smoothed image, 0.14 counts s^{-1} $arcmin^{-2}$. The Honeycomb Nebula is the source at $5^h35^m44^s$, −69°17′56″ (J2000), and the SN 1987A is the source at $5^h35^m28^s$, −69°16′12″ (J2000).

available to us. The X-ray software package PROS[2] was used to analyze these *ROSAT* data.

Figure 1(a) displays a smoothed X-ray image, and Fig. 1(b) an Hα image overlaid by X-ray contours. The X-ray image is produced from the event file of the *ROSAT* PSPC observation rp500100 over the energy range 0.1–2.4 keV. The data array is first blocked by a factor of 10 to get 5″ pixels, then smoothed by a Gaussian function with σ=3 pixels. This procedure improves the signal-to-noise ratio, but does not excessively degrade the spatial resolution of 30″. The Hα picture is produced from a PDS scan file of a photographic plate taken with the Curtis Schmidt Telescope (Kennicutt & Hodge 1986); its resolution is limited by the scanning aperture of 5″. The Honeycomb Nebula appears as a broad, inconspicuous filament in this low-resolution Hα picture.

The Honeycomb Nebula is coincident with the bright X-ray source at $5^h35^m44^s$, −69°17′56″ (J2000). There is faint diffuse X-ray emission near the Honeycomb, but this emission is not bounded by any identifiable shell structure in the Hα image. In fact, diffuse X-ray emission is visible throughout the field shown in Fig. 1, but no optical counterparts can be unambiguously identified. The only exceptions are the bright source at the NE corner–the known SNR 30 Dor B (Mathewson *et al.* 1983; Chu *et al.* 1992; Dickel *et al.* 1994), and the prominent shell structure at the north—the supershell 30 Dor C (Mathewson *et al.* 1985; Chu & Kennicutt 1988).

The *ROSAT* HRI observation unfortunately could not resolve the loop structure in the Honeycomb; the instrumental FWHM is comparable in size to each loop and the image shows only diffuse emission. No prominent point source or bubble structure is evident.

Spectral properties of the Honeycomb can be extracted from the PSPC observation. We define a source region encompassing the emission from the Honeycomb and a background region off the source, then subtract the background contribution to extract a spectrum of the Honeycomb itself. However, it is not easy to define a "background" region in such a complex environment. We have selected two background regions, one includes the diffuse emission at ∼2′ south of the Honeycomb to represent a "high" background, and the other includes the faintest region at ∼7′ northwest of 30 Dor C to represent a "low" background. Within a source region of 2 $arcmin^2$, 575 counts are registered. The net source counts are 467±24 and 309±26 for the low and high backgrounds, respectively. The corresponding source-count rates are 0.017±0.001 and 0.011±0.001 counts s^{-1}.

The background-subtracted PSPC spectrum of the Honeycomb (Fig. 2) is very soft, with most of the counts below 1 keV. We have fitted Raymond & Smith (1977) plasma emission models with Morrison & McCammon (1983) absorption to the spectra, allowing both plasma temperature and absorbing column density N_H to be fitted as free parameters. The χ^2 grid (Fig. 3) indicates that at 99% level of confidence the plasma temperature kT=0.1–0.6 keV and the absorbing column $\log N_H$=22.0–20.5; the minimum χ^2=15 occurs for kT =0.33 keV and $\log N_H$=21.06. This small amount of absorbing column density is similar to what is found toward SN 1987 A, $\log N_H$=21.3 (Savage *et al.* 1989). The best-fit Raymond and Smith model is plotted in dashes over the spectrum in Fig. 2. The X-ray luminosity calculated from the best-fit model is 7×10^{34} erg s^{-1} in the 0.5–2.0 keV band.

The X-ray luminosity derived from the PSPC observation can be compared to that derived from the *Einstein* IPC observation. The usual conversion of 1 IPC counts

[2]PROS is developed, distributed, and maintained by the Smithsonian Astrophysical Observatory, under partial support from NASA Contracts No. NAS5-30934 and No. NAS8-30751.

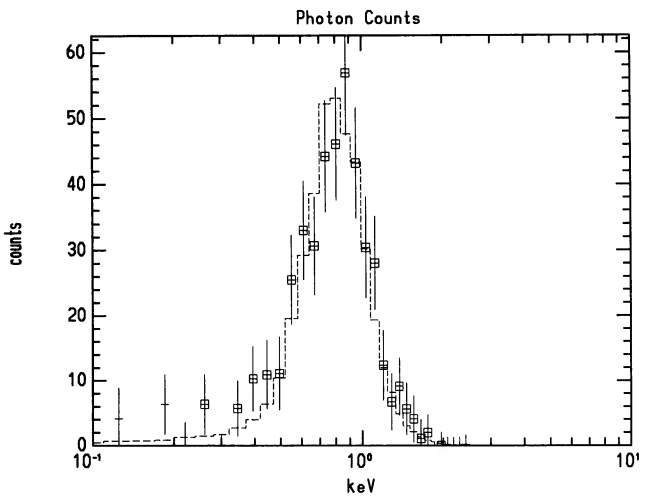

FIG. 2. *ROSAT* PSPC spectrum of the Honeycomb Nebula. The dashed curve is a Raymond and Smith model with $\log N_H=21.06$ and $kT=0.33$ keV.

$s^{-1}=2\times10^{37}$ erg s^{-1} in the LMC (Long *et al.* 1981) should not be used because the plasma temperature of the Honeycomb is much lower than the 5×10^6 K (or 0.45 keV) assumed in this conversion formula. Using the conversion factor for $\log N_H=21.06$ and $kT=0.33$ keV (derived from the *ROSAT* PSPC data) in Fig. 5A.12 of the *Einstein Observatory* Revised User's Manual, the observed IPC count rate of 0.01 counts s^{-1} (Wang & Helfand 1991) corresponds to an X-ray luminosity of 1.1×10^{35} erg s^{-1} in the *Einstein Observatory* band of 0.2 to 4.0 keV. This is consistent with the PSPC results.

In the *ROSAT* HRI image, 160±25 source counts (background subtracted) were detected within a 2 arcmin^2 elliptical aperture, corresponding to a count rate of 0.0068±0.0011 counts s^{-1}. The ratio of our measured HRI to PSPC count rate is consistent with the instrumental characteristics reported in the Addendum of Appendix F of the *ROSAT* Mission Description—the PSPC count rate being roughly 2.5–3.3 times the HRI count rate.

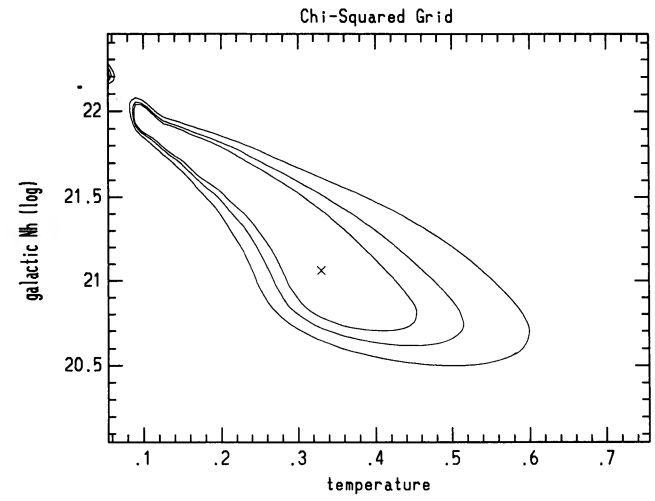

FIG. 3. χ^2 grid plot for the Raymond and Smith model fits to the Honeycomb's spectrum. The three contours correspond to 68%, 90%, and 99% confidence levels.

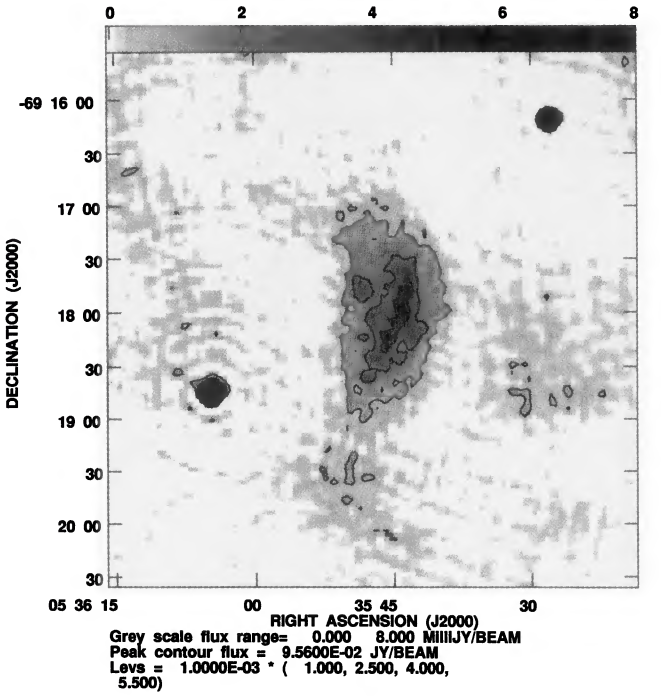

FIG. 4. An AT Compact Array map of the Honeycomb at 1420 MHz. The resolution is 6.″4. The two bright sources are SN 1987A at the northwest and an unidentified background source at the southeast.

3. RADIO PROPERTIES OF THE HONEYCOMB

In the 843 MHz radio map made with the Molonglo Observatory Synthesis Telescope (MOST; Mills & Turtle 1984), the Honeycomb Nebula is clearly detected with a peak flux density of 60 mJy per 43″×46″ beam. This bright radio emission is most likely synchrotron radiation rather than thermal, since it has a much higher radio/optical ratio than the nearby H II regions in Fig. 1(b). For example, compared to the bright ring structure adjacent to the southwest rim of 30 Dor C, the Honeycomb Nebula is a factor of 2–3 fainter in Hα but a factor of 3 brighter at 843 MHz. There is faint radio emission extending from the Honeycomb toward the west and southwest, forming a circular arc structure. The nature of this radio extension will be discussed later in Sec. 5.

Maps at three frequencies—1420, 4800, and 8640 MHz—were made with the Compact Array of the Australia Telescope. The primary calibration source was PKS B1934−638 with flux densities of 14.9, 5.8, and 2.8 Jy, respectively. The secondary phase calibrators were PKS B0407−658 and PKS B0530−727. The map at 1420 MHz was made with seven different antenna configurations between 1993 January and 1994 February. These observations were taken during the course of a mosaic of the 30 Doradus region and regular monitoring of SN 1987A. The total data set has good *uv* coverage out to the longest baseline of 6 km, resulting in a half-power beamwidth of 6.″4. The final 1420 MHz map is shown in Fig. 4; the bright point source at the northwestern corner is SN 1987A, and the bright source east of the south-

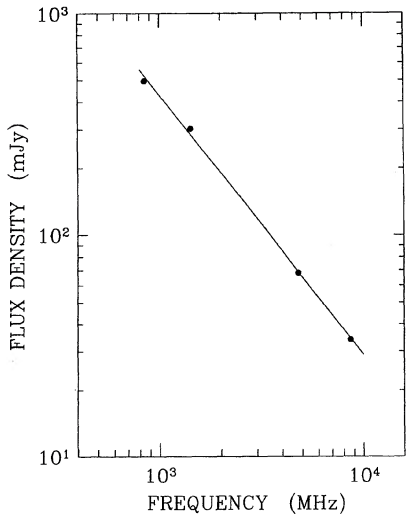

FIG. 5. Plot of log (flux density) vs log (frequency) for the Honeycomb Nebula. The best fit is overplotted, and its slope is −1.17.

ern end of the Honeycomb is an unidentified background source. As shown in Sec. 4, the radio image shows an excellent correlation with the honeycomb structure. The resolution is insufficient to make out individual loops; nevertheless, the radio image peaks along the prominent optical loops, while the extended radio plateau corresponds to the less well-defined loop structures. In Wang's (1992) centerfold picture of the Honeycomb, there are "chain link" structures, extending from the northern end of the Honeycomb toward the northeast. These chain-link structures show the faint radio counterpart in Fig. 4. There are also hints of faint extended structure to the west and southwest of the Honeycomb in the 1420 MHz map.

At 4800 and 8640 MHz, observations were taken with the 0.375 km configuration of the Compact Array on 1994 April 5, resulting in half-power beamwidths of 26.″5×14.″3 at position angle 11°, and 18.″0×8.″6 at position angle 17°, respectively. These beams are too large to reveal any of the detailed honeycomb structure, but do show the overall outline of the source and can be used to obtain the integrated flux densities. The difficulty with getting good flux densities is the removal of the background emission that varies over the source area. The background can also be a function of frequency because it may have a different spectral index than the SNR, and also because the aperture synthesis observations did not have identical scaled antenna separations at each frequency. We were successful in choosing an identical area to the east of the nebula, which had a consistent relative level on all the maps. Any error will thus bias all the flux densities by the same ratio and so the derived spectrum should be accurate. The total flux densities integrated over the Honeycomb Nebula were 496 mJy at 843 MHz, 303 mJy at 1420 MHz, 68 mJy at 4800 MHz, and 34 mJy at 8640 MHz. These values are plotted in Fig. 5. The resultant spectral index, α, in flux density $S_\nu \propto$ (frequency)$^\alpha$, is −1.17. Such a number indicates definite nonthermal emission, but with a slope considerably steeper than that for most shell SNRs. The southwestern extension is too faint to determine a reliable spectral index, but it does not appear relatively brighter at the higher frequencies and is likely also nonthermal.

4. OPTICAL IMAGING OF THE HONEYCOMB NEBULA

To complement our X-ray and radio data, and to augment our multiwavelength coverage, we also obtained optical images of the nebula in the emission lines of Hα, [S II], and [O III]. The ratio of the [S II] to Hα flux is a sensitive diagnostic of the nature of the emission mechanism. The shocked gas in SNRs typically exhibits [S II]/Hα ratios greater than 0.4, while photoionized gas, such as that in H II regions, usually displays ratios of ~0.1, because the sulfur is kept in the S^{++} state by the continuous flow of ionizing photons. While Wang (1992) reported that the loops in the Honeycomb Nebula were seen in both Hα and [O III] images, no [S II] observations have been reported.

The optical images were taken with the University of Michigan/CTIO Curtis Schmidt telescope on 1994 February 19 UT. A Thomson 1024×1028 CCD was mounted at the Newtonian port, giving a scale of 1.″835 pixel^{-1} and a field of view of 31.′3. Narrow-bandpass filters centered on Hα (λ_c=6564 Å, $\Delta\lambda$=20 Å), [S II] (λ_c=6724 Å, $\Delta\lambda$=50 Å), and [O III] (λ_c=5010 Å, $\Delta\lambda$=50 Å) were used to isolate the nebular emission, and a red continuum filter (λ_c=6840 Å, $\Delta\lambda$=95 Å) was used to obtain images of the continuum background. Multiple frames were obtained through each filter, amounting to total integration times of 800 s in Hα, 2400 s in [S II], 1200 s in [O III], and 600 s in the continuum. The data were reduced with IRAF,[3] and multiple frames were shifted and combined to obtain the images shown in Fig. 6.

The resolution of our optical observations is not as high as that of Wang's (1992) discovery images; however, the loops for which the nebula was named are apparent in the images. The [S II] images are compared to the radio 1420 MHz map in Fig. 7. The correlation between radio peaks and the loop structure is evident.

It is clear from the comparison of the Hα and [S II] images that the nebula exhibits strong [S II] emission relative to the brighter Hα filaments in the vicinity. However, as with both the X-ray and radio data, the complex environment of this nebula makes removal of the background emission difficult, thus making the calculation of a [S II]/Hα ratio problematic. We first made a "ratio" map from the [S II] and Hα images by simply sky subtracting the images (based on sky levels determined 15′ to 20′ to the west), clipping both images at three times the sky standard deviation, and dividing the two images. This ratio map is shown in Fig. 6(d), together with the Hα, [S II], and [O III] images. The "raw" [S II]/Hα ratio for the filaments determined in this way is between 0.3 and 0.4, just below the nominal dividing line for shocked gas (typically 0.4; see Long *et al.* 1990 and references therein). However, this low ratio is not unexpected, given the strong contamination by the underlying Hα emission from the background (or foreground) H II region.

[3]IRAF is distributed by the National Optical Astronomy Observatories (NOAO).

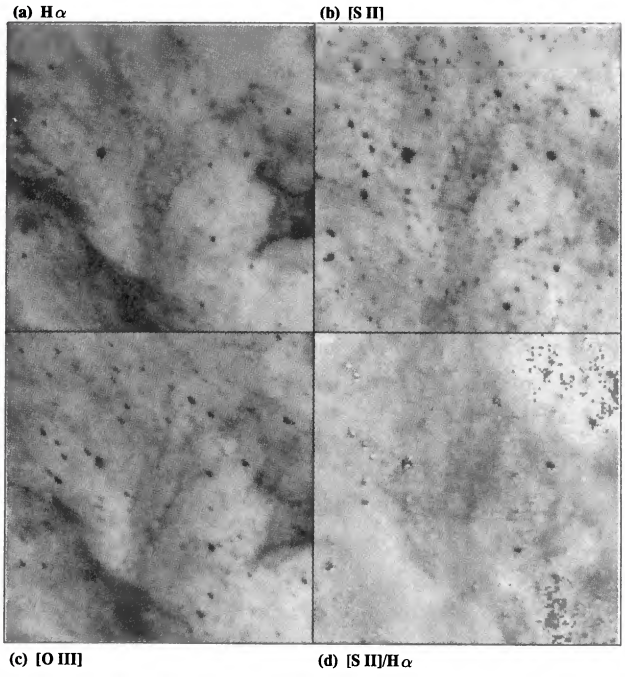

FIG. 6. Curtis Schmidt CCD images of the Honeycomb Nebula and its vicinity in (a) Hα line, (b) [S II] line, (c) [O III] line, and (d) [S II]/Hα ratio. The field of view is 3.'9×3.'9. The field center is roughly $5^h35^m45^s$, $-69°18'15''$ (J2000).

To try to derive a more accurate ratio for the filaments themselves, we attempted to subtract the local background and recalculate the [S II]/Hα ratios at various locations in the nebula. We calculated a mean sky value from ten 30 arcsec^2 apertures (3×3 pixels) scattered evenly around the nebula. We then used the same apertures to measure the mean flux of six filaments. Subtracting the mean sky values from the [S II] and Hα fluxes, we derived background-corrected [S II]/Hα ratios of from 0.41 to 0.55. Using individual estimates of the background emission, the estimates of the ratios of the brighter filaments ranged up to 0.67. While the uncertainties in the derived ratios are large ($\pm$0.2), they substantiate an enhancement of [S II] emission in the nebular filaments, which is indicative of SNR activity. Accurate spectroscopy is needed before we can make more serious comparison to models.

5. THE HONEYCOMB NEBULAR AS A SUPERNOVA REMNANT

The bright X-ray emission, nonthermal synchrotron radiation, enhanced [S II]/Hα ratios, and fast shocked gas detected in the Honeycomb Nebula all suggest a SNR. However, the Honeycomb is different from the run-of-the-mill SNRs; most notably, it does not have a coherently expanding shell structure. The absence of a complete shell structure indicates that the supernova must have exploded in a low-density medium, and the Honeycomb is produced by the blast wave colliding with a dense sheet of gas (Meaburn *et al.* 1993, 1995). This mechanism is similar to what has been proposed to explain the excess X-ray emission in superbubbles in the LMC (Chu & Mac Low 1990). The interaction could be quite recent. In general, young remnants have steeper spectra than older ones (e.g., Dickel 1991), and so the steep value of the spectral index for the Honeycomb could represent the very early acceleration of relativistic particles that have not yet had a chance to build up their low-energy component through stochastic acceleration processes (Cowsik & Sarkar 1984).

This formation mechanism is consistent with the observed X-ray and kinematic properties of the Honeycomb. In the Sedov (1959) solution, the post-shock temperature for a fully ionized plasma consisting of 65% H and 35% He would be

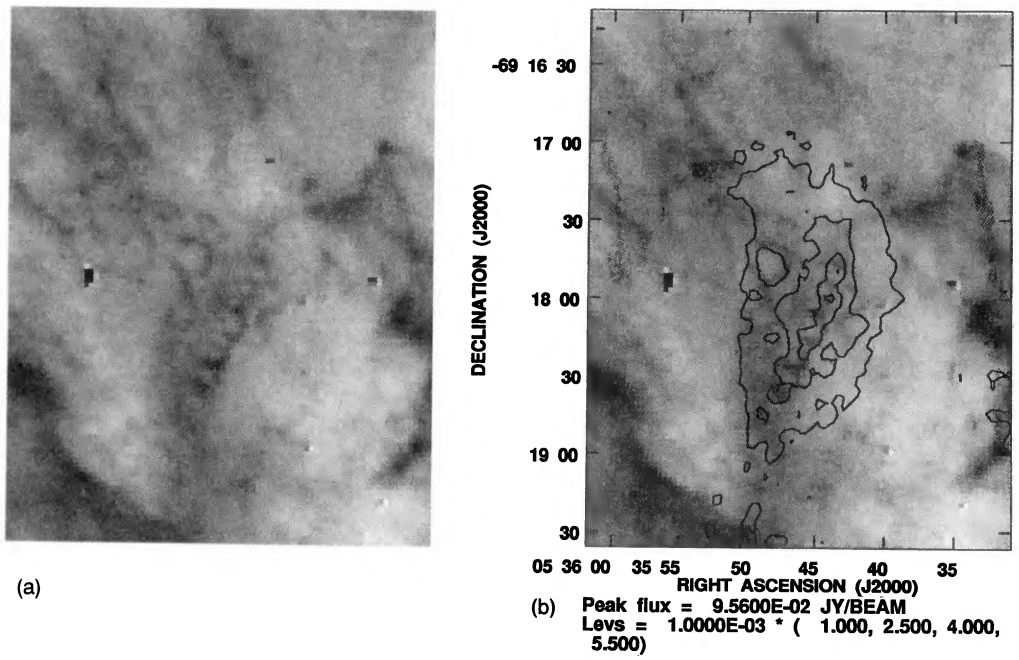

FIG. 7. (a) Curtis Schmidt CCD image of the Honeycomb Nebula in [S II], (b) 1420 MHz radio contours overlaying the [S II] image.

$kT=0.0125\ V_{100}^2$ keV, where V_{100} is the shock velocity in 100 km s^{-1}. The Hα expansion velocity of 300 km s^{-1} (Meaburn *et al.* 1995) implies a shock velocity of 400 km s^{-1} (for adiabatic shocks, shock velocity=4/3 of the expansion velocity), and the post-shock plasma temperature would be 0.2 keV, or 2.2×10^6 K. However, the SNR shock may not be directed along the line of sight. If the shock is at 45° to the line of sight, the real shock velocity will be 565 km s^{-1} and the post-shock temperature will be 0.4 keV, or 4.4×10^6 K. This is in excellent agreement with the plasma temperature indicated by the PSPC spectrum.

The kinematic observations of the Honeycomb (Meaburn *et al.* 1993, 1994) provide many clues to the geometry and physical condition of the SNR shocks. The predominantly blue-shifted shock velocities require that the supernova be on the far side of the dense sheet of gas. The rapid velocity variation, forming many expanding hemispherical structures, indicates that the dense sheet of gas must be porous. A faint, extended, red-shifted component is detected by Meaburn *et al.* at V_{hel}=338 to 348 km s^{-1}, but no counterpart is present in the interstellar absorption against the UV spectrum of SN 1987 A (Savage *et al.* 1989). Therefore, this red-shifted component must be from the far side of the dense sheet, as well as the Honeycomb itself, and could be the receding side of the large shell surrounding the low-density medium. A similar condition has been seen in the SNR 30 Dor B, in which a faint, extended, red-shifted component is detected at areas where the receding side of the SNR is absent (Chu *et al.* 1992). Unfortunately, the spatial coverage of the kinematic observation of the Honeycomb was not adequate to define the boundary of the large surrounding shell, and without this information it is impossible to identify the shell structure in the Hα images in Figs. 1 and 7.

We may derive information about the interstellar environment of the Honeycomb by comparing the radio, optical, and X-ray images over a large scale. In Fig. 1(b), the X-ray contours show a ridge of X-ray emission along a long Hα filament extending from the northeast toward the southwest of Honeycomb. The 1420 MHz map in Fig. 4 shows faint emission along this long filament, with an apparent break to the southwest of the unidentified background radio source at $5^h36^m05^s$, $-69°18'40''$ (J2000). This long filament might have been hit by shocks from the same SNR. However, the southwestern end of this long filament is also part of the circular arc structure seen in the MOST 843 MHz map (Mills & Turtle 1984). This arc structure can be seen in the 1420 MHz map in Fig. 4, where, compared to 843 MHz, it appears to be nonthermal. It is not clear whether the Honeycomb Nebula is closely associated with the circular radio arc extending toward the west and southwest (Fig. 4) or with the long optical/X-ray filament [Fig. 1(b)].

The Honeycomb SNR demonstrates the difficulty in piecing together a complete story of a SNR in a complex environment that has had multiple supernova events over several million years. Its presence indicates the coexistence of hot, low-density medium and a cold, dense sheet of gas, although no information on the relative filling factor can be obtained. It is conceivable that many more SNRs similar to the Honeycomb are still hidden in complex star-formation regions, and careful analysis of soft, diffuse X-ray emission would be the first step to uncover these SNRs.

We thank Andrew Reid and Ross Beyer for help with the data reduction, and R. C. Kennicutt for providing the PDS scan file of his Hα plate. Y.H.C. acknowledges the support of NASA Grants No. NAG 5-1900, No. 5-2112, and No. 5-2679. J.R.D. acknowledges the Campus Honors Program of the University of Illinois and NASA Grant No. HST AR 5295.01-93A.

REFERENCES

Chu, Y.-H., & Kennicutt, R. C. 1988, AJ, 95, 1111
Chu, Y.-H., Kennicutt, R. C., Schommer, R. A., & Laff, J. 1992, AJ, 103, 1545
Chu, Y.-H., & Mac Low, M.-M. 1990, ApJ, 365, 510
Cowsik, R., & Sarkar, S. 1984, MNRAS, 207, 745
Dickel, J. R. 1991, in Santa Cruz Summer Workshop in Astronomy and Astrophysics, Supernovae, edited by S. E. Woosley (Springer, New York), p. 675
Dickel, J. R., Milne, D. K., Kennicutt, R. C., Chu, Y.-H., & Schommer, R. A. 1994, AJ, 107, 1067
Kennicutt, R. C., & Hodge, P. W. 1986, ApJ, 306, 130
Long, K. S., Blair, W. P., Kirshner, R. P., & Winkler, P. F. 1990, ApJS, 72, 61
Long, K. S., Helfand, D. J., & Grabelsky, D. A. 1981, ApJ, 248, 925
Mathewson, D. S., Ford, V. L., Dopita, M. A., Tuohy, I. R., Long, K. S., & Helfand, D. J. 1983, ApJS, 51, 345
Mathewson, D. S., Ford, V. L., Tuohy, I. R., Mills, B. Y., Turtle, A. J., & Helfland, D. S. 1985, ApJS, 58, 197
Meaburn, J., Wang, L., & Bryce, M. 1995, A&A, 293, 532
Meaburn, J., Wang, L., Palmer, J., & Lopez, J. A. 1993, MNRAS, 263, L6
Mills, B. Y., & Turtle, A. J. 1984, in IAU Symposium No. 108, Structure and Evolution of the Magellanic Clouds, edited by S. van den Bergh and K. de Boer (Reidel, Dordrecht), p. 283
Morrison, R., & McCammon, D. 1983, ApJ, 270, 119
Pfeffermann, E. *et al.* 1987, Proc. SPIE, 733, 519
Raymond, J. C., & Smith, B. W. 1977, ApJS, 35, 419
Savage, B. D., Jenkins, E. B., Joseph, C. L., & de Boer, K. S. 1989, ApJ, 345, 393
Sedov, L. 1959, Similarity and Dimensional Methods in Mechanics (Academic, New York)
Wang, L. 1992, ESO Messenger, No. 69, 34
Wang, Q., & Helfand, D. J. 1991, ApJ, 370, 541